Time-Expanded ΦOTDR Based on Orthogonal Polarization Frequency Comb Generation

Pascual Sevillano, Javier Preciado-Garbayo, David Izquierdo, Miguel Soriano-Amat, Sonia Martin-Lopez, *Member, IEEE*, Miguel Gonzalez-Herraez, *Senior Member, IEEE*, and María R. Fernández-Ruiz

***Abstract*—Phase-sensitive Optical Time-Domain Reflectometry (ΦOTDR) has emerged as an effective and high-performance solution within the realm of Distributed Optical Fiber Sensing (DOFS) technologies, which has promoted its use in an ever-growing number of fields. The challenges arisen by new operation fields demand surpassing the historical trade-offs in this technology, specially aiming for higher resolution without jeopardizing the system simplicity and cost-effectiveness. In this context, time-expanded (TE-)ΦOTDR has been recently proposed as a DOFS solution delivering cm-range resolution with sub-MHz detection and acquisition bandwidths. It is based on the use of an interferometric scheme that employs a dual frequency comb (DFC), consisting of two mutually coherent optical frequency combs with dissimilar repetition rates. In this paper, we present a novel DFC generation scheme for TE-ΦOTDR that exploits the polarization orthogonality. In particular, our approach considerably increases the common path followed by the two frequency combs, thus reducing instability and noise as compared to the conventional generation scheme. Additionally, we employ an IQ modulation scheme with two PRBS generators that increases the scalability of the interrogator while severely reducing its cost and complexity. Results show a reduction in the noise amplitude spectral density especially at low frequency values, which corroborates the stability enhancement of this proposed architecture as compared to the conventional scheme.**

***Index Terms*—Dual frequency comb, optical time-domain reflectometry, rayleigh scattering, structural health monitoring.**

Manuscript received 26 January 2024; revised 26 March 2024 and 19 April 2024; accepted 28 April 2024. Date of publication 2 May 2024; date of current version 16 September 2024. The work of Miguel Soriano-Amat was supported in part by MCIN/AEI/10.13039/501100011033 and in part by FSE invierte en tu futuro under Grant PRE-2019–087444. The work of María R. Fernández-Ruiz was supported in part by MCIN/AEI/10.13039/501100011033 and in part by Unión Europea «NextGenerationEU»/PRT under Grant RYC2021-032167-I. This work was supported in part by the Diputación General de Aragon under Grant T20_23R, in part by the Spanish Research Agency under ICR100G project under Grant PID2020-114916RB-I00, in part by Spanish the Ministry of Science and Innovation (MICINN) through RTC under Grant DI-17-09169, in part by the Spanish MCIN/AEI/10.13039/501100011033 and the European Union NextGenerationEU/PRTR Program under Grant PSI ref. PLEC2021-007875 and Grant TREMORS ref. CPP2021-008869, in part by the Spanish MCIN/AEI/10.13039/501100011033, and in part FEDER under Grant PID2021-128000OBC21, Grant PID2021-128000OB-C22, and Grant PID2022-140963OA-I00, in part by the European Innovation Council under Grant SAFE: ref. 101098992 and the Grant SUBMERSE ref.101095055, in part by the CETPartnership, under the 2022 joint call, co-funded by the European Commission under Grant GA N°101069750, and in part by MCIN/AEI/10.13039/501100011033, Project SEASNAKE+, ref: CETP2022-00371. *(Corresponding author: Pascual Sevillano.)*

Pascual Sevillano and David Izquierdo are with the Photonic Technologies Group (GTF), Aragon Institute of Engineering Research (I3A), Universidad de Zaragoza, 50018 Zaragoza, Spain (e-mail: psevi@unizar.es; d.izquierdo@unizar.es).

Javier Preciado-Garbayo is with the Photonic Technologies Group (GTF), Aragon Institute of Engineering Research (I3A), Universidad de Zaragoza, 50018 Zaragoza, Spain, and also with the Company Aragon Photonics Labs S.L., 50009 Zaragoza, Spain (e-mail: j.preciado@aragonphotonics.com).

Miguel Soriano-Amat, Sonia Martin-Lopez, Miguel Gonzalez-Herraez, and María R. Fernández-Ruiz are with the Universidad de Alcalá, 28805 Alcalá de Henares, Spain (e-mail: miguel.soriano@uah.es; sonia.martinlo@uah.es; miguel.gonzalezh@uah.es; rosario.fernandezr@uah.es).

Color versions of one or more figures in this article are available at https://doi.org/10.1109/JLT.2024.3396221.

Digital Object Identifier 10.1109/JLT.2024.3396221

I. Introduction

PHASE-SENSITIVE Optical Time-Domain Reflectometry (ΦOTDR) has become one of the most employed Distributed Optical Fiber Sensing (DOFS) techniques nowadays [1], [2], [3]. The rapid developments experienced in the last decade have been driven by its increasing applicability to a broad range of fields, from third party intrusion detection to seismic monitoring. Besides, a growing demand to provide higher spatial resolution and higher sensitivity has been promoted by research towards new applications, including shape sensing, transportation monitoring and more [4], [5], [6]. ΦOTDR is based on the analysis of the Rayleigh backscattering of pulses with high coherence and high peak-power propagating along an optical fiber. Local variations in the refractive index of the fiber caused by thermal or mechanical stress in its vicinity alter this backscatter, so that it is possible to detect such variations. Using direct detection schemes, the analysis of intensity changes in consecutive backscattered traces can reveal and locate these perturbed spots along the fiber [7]. However, these schemes often exhibit poor sensitivity and lack fidelity or linearity to the applied perturbation [8]. On the other hand, coherent detection schemes recover the phase of the backscatter trace, boosting the sensing range and enhancing the sensitivity. Despite the improvement in range, these techniques exhibit reduced long term-stability, making them unsuitable for scenarios with quasi-static perturbations, such as deformation monitoring for critical infrastructures [9]. On the other hand, enhancing the spatial resolution in ΦODTR systems requires employing shorter pulses and higher peak-power probe pulses, but it is limited by the appearance of unwanted nonlinear effects, such as modulation instability [10]. Approaches employing any kind of modulation format on the probe pulse to reduce the peak power have been also presented to improve the resolution [11], [12]. However, they require very broad detection and acquisition bandwidths, not only severely increasing the detection induced noise but also

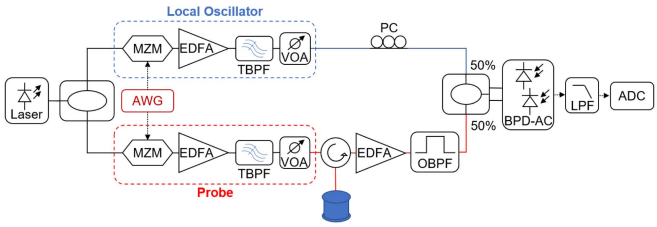

Fig. 1. Conventional scheme of a TE-ΦOTDR. VOA: Variable optical attenuator. LPF: low-pass filter. ADC: analog-to-digital converter. The remaining acronyms are explained within the text.

the cost and complexity of the system. A few years ago, a novel technique named time-expanded (TE-)ΦOTDR was introduced to partly mitigate these requirements. This technique allows centimeter resolutions with similar sensitivity to conventional ΦOTDR techniques [13].

TE-ΦOTDR is based on a coherent scheme that employs two mutually coherent optical frequency combs (OFCs) with a slight difference in their repetition rate acting as local oscillator (LO) and probe, respectively. Mixing the backscattered signal from the probe with the LO induces a multiheterodyne process that downconverts the optical traces to the radio frequency (RF) domain. This downconversion dramatically reduces the bandwidth requirements in the detection stage, enabling high spatial resolutions (<5 cm) with MHz bandwidth detectors [14]. The use of smart spectral phase coding in the combs generation prevents nonlinear effects without impairing the sensitivity at no processing cost, as long as probe and LO combs share the same phase coding [15]. However, the generation of this tailor-made signals requires complex generation stages with costly arbitrary waveform generators (AWG) as the cornerstone. Although this requirement has been overcome in recent works by the use of inexpensive pseudorandom binary sequence (PRBS) generation boards [16], or field-programmable gate arrays (FPGA) [17], the system still requires highly-precise timing and synchronization; two optical modulators, one for each comb; and two extremely sharp Tunable Optical Bandpass Filters (TBPF) to obtain optical single side band (OSSB) signals.

These constrains reduce the scalability of the system, being limited by the performance of the aforementioned components, and limit its integration for real field scenarios. Furthermore, the previously indicated frequency downconversion reduces the attainable acquisition rates which increase the measurement times. This effect added to the independent modulation of each branch where thermal and mechanical noise can affect with different intensity and time dependence, impair the stability of the system, specially for long-term measurements [18].

In this work, we introduce and evaluate an innovative probe/LO generation stage for TE-ΦOTDR that enhances the stability of the measurement compared to the conventional generation scheme and, at the same time, reduces its complexity. The scheme relies on the generation of both LO and probe signals on a single electro-optical modulator, leveraging the two orthogonal states of polarization (SOP). Hence, the two signals share a common path from the generation stage to the sensing region where they must be split. For that purpose, we employ a Dual-Pol IQ modulator, that not only ensures the orthogonality of the combs in its generation but it also allows for the direct generation of the OSSB by using 90° hybrids that drive the IQ branches of each polarization. Additionally, we employed cost-effective PRBS boards that replace the AWG and eliminate the need for generating long tailor-made complex envelope signals for the combs as described in [16]. By using this architecture, we reduce the number of elements in the transmitter and increase its capability to be integrated and scaled in order to be employed in real field scenarios. While the novel generation stage was initially presented in [19], in this work we have evaluated the long-term stability of the system by performing longer measurements. Furthermore, our investigation centers on quantifying the performance enhancement derived from this novel scheme. To achieve this, we conducted a comparative analysis of the proposed generation scheme against the conventional approach, specifically focusing on sensitivity. Moreover, spectral analysis of the noise proves a significant reduction in the low frequency region, which demonstrate the enhancement in the stability of long-term measurement when using the proposed common-path generation scheme.

II. TE-Phi OTDR Architecture

A. Measurement Principle

The TE-ΦOTDR measurement principle is based on the use of two frequency combs with the same amplitude and phase information in their N lines. The only difference between both combs is their repetition rate, fr, that presents a slight difference, $\delta f << fr$. One of the combs is used as LO, and the other one as probe, which interrogates the fiber under test (FUT). The backscattered signal of the probe coming from the FUT beats with the LO in a photodiode, generating an electrical frequency comb.

The frequency line spacing of the electrical comb is the frequency difference between the original optical combs, δf, resulting in a reduced bandwidth signal compared to the optical ones. In this way, the bandwidth required for detection is considerably lower. In the TE-ΦOTDR schemes shown in the literature, the bandwidth of the original combs is in the GHz range, their line spacing is of MHz, and the spacing difference in the 10's Hz-kHz regime. The detected new comb has 10's Hz-kHz line spacing and a total bandwidth of in the MHz range. The ratio between the optical and the electrical bandwidths, namely the compression factor (CF), has typical values that ranges from 10^3 to 10^5 s [13].

B. Conventional Signal Generation Scheme

In the conventional scheme, shown in Fig. 1, the frequency combs are digitally generated using two AWG or a two-channel AWG. The frequency combs are generated in the spectral domain as a double sideband signal by precisely controlling the amplitude and phase of their spectral lines, the number of lines that compose the combs (N), repetition rate (f_r) and the frequency shift between probe and LO repetition rates (δf). Subsequently,

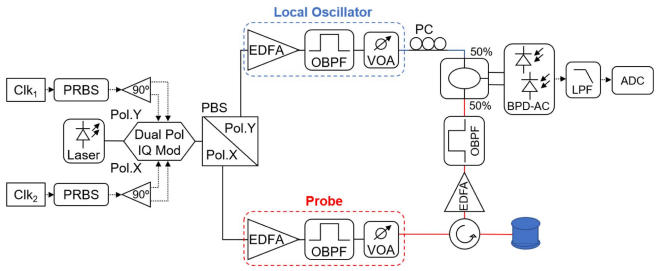

Fig. 2. Proposed alternative scheme of TE-ΦOTDR based on a common path probe/LO generation using orthogonal polarization frequency combs.

these combs are transformed into the time domain through an inverse Fourier transform. The resultant real-valued electrical signals drive two Mach-Zehnder Modulators (MZMs), both fed with the same narrow linewidth laser to ensure their mutual coherence. The output signals of both MZM are amplified by Erbium-Doped Fiber Amplifiers (EDFAs). Then, the amplified signals are filtered with two extremely sharp Tunable Optical Bandpass Filters (TBPFs) to reject one of the modulated bands in the optical spectrum, as well as to reduce the Amplified Spontaneous Emission (ASE) from the EDFAs. This step is crucial for the system performance, as it needs Optical Single-Sideband (OSSB) frequency combs to guarantee an unambiguous frequency downconversion. Once both signals are converted to OSSB signals, the probe is injected into the FUT. Then, the backscattering signal is amplified, filtered with an Optical Bandpass filter (OBPF) and then coupled to the LO. The interference between backscattered signal and LO is detected by a pair of balanced photodiodes (BPDs). This signal mixing in the BPDs generates the low-frequency, compressed comb that is digitalized and processed afterwards.

C. Alternative Scheme Based on Common Path Comb Generation

The proposed novel scheme, shown in Fig. 2, has a simplified alternative to the transmitter stage used in the conventional scheme. This configuration offers higher scalability and long-term stability in the measurement by replacing the AWGs and the two MZMs by two PRBS generators and a dual-polarization (Dual-Pol) IQ modulator. In this scheme, the electrically modulated frequency combs are not digitally composed in the frequency domain, but it rather takes advantage of the spectral characteristics of the PRBS sequences. The spectrum of a PRBS pattern is a sequence of N peaks, spaced in the frequency domain by R_b/N, where R_b is the bit-rate (R_b) of the sequence and N represents also its length. The length of this pattern is determined by the size of the linear feedback shift register (LFSR) employed in its hardware generation. The length of the PRBS is often expressed as $N = 2^{k-1}$ bit sequence where k is the order of the sequence, corresponding to the order of the feedback polynomial. This extremely simplifies the signal generation stage, which now produces periodic pulse patterns in time-domain, allowing an increase of SNR similar to that achieved in TE-ΦOTDR with random spectral phase modulation [8]. Besides, it can be simply tuned by changing the bit-rate and the length of the sequence with no limit, in principle, in the sequence length. This leads to an important advantage with respect to the use of an AWG, in which the sequence length is limited by its memory depth [16].

In the proposed architecture, the Dual-Pol IQ modulator enables the direct generation of OSSB signals without optical filtering and the generation of the two combs in the same modulator using orthogonal polarizations. A standard IQ modulator permits the generation of complex modulation formats using two branches, each consisting in two independent Mach-Zehnder modulators (MZM), the in-phase arm (I) and the quadrature arm (Q), which are combined with precise phase control between them to ensure their orthogonal combination. To maintain the modulator operation point over long-term periods, the bias voltages are regulated using a commercial automatic bias controller. This controller stabilizes the operation point by tapping 1% of the modulated signal. A Dual-Pol IQ modulator, in turn, integrates two IQ modulators whose outputs are combined with a polarization beam combiner obtaining an output signal with two orthogonal polarizations, commonly named X and Y. To obtain an OSSB signal with IQ modulators, the combination of the I and Q modulation signals must result in an analytic signal. It is usually made by the Hilbert transform. For this purpose, in our approach, we use 90° electric hybrid couplers that provide a half power copy of the input signal and its 90° phase shifted copy, i.e., its Hilbert transform. These two phase-shifted signals, when connected to the IQ modulator, generate the desired OSSB modulation. This common-path based generation uses orthogonal SOP to mitigate the stability issues present in conventional two-path interferometers. This present a meaningful advantage in front of the conventional scheme, in which the LO and probe generation branches are exposed to different environmental noise and fluctuations which in turn increases the undesired noise. Moreover, IQ-modulators are widely used in optical communications with rates higher than 40 GHz and enable complex modulation formats that open the possibility to a wider use of the spectrum.

Once the two orthogonal polarization OSSB signals are generated simultaneously in the dual-Pol IQ modulator, they are separated by a polarization beam splitter (PBS) to obtain the LO and probe signals. Both signals, as in the conventional scheme, are boosted up by EDFAs and filtered using conventional OBPFs to filter out the ASE prior to the coupling of the probe into the sensing fiber through the circulator. Note that, with this direct generation of the OSSB with the IQ modulator, the role of the filters is merely to filter-out the ASE generated by the EDFAs. This contrasts with the conventional scheme, where filters must have a particularly high roll-off and require precise tuning at the edge to match the carrier frequency, aiming to reject one of the sidebands without impacting the other. Moreover, this method of OSSB generation also mitigates the risk of impairments due to relative wavelength misalignment between the filter and the signal, a potential issue in long-term measurements due to thermal fluctuations. The detection stage is similar than the one used in the conventional scheme.

III. Results and Discussion

A. Experimental Setup

The optical source employed in our setup is a highly coherent continuous-wave laser with a linewidth <0.1 kHz emitting at 1550.12 nm that directly feeds the Dual-Pol IQ modulator, in the proposed scheme, or the coupler before the MZMs, in the conventional scheme. The OBPFs used after the EDFAs to reduce the ASE are DWDM filters with 100 GHz optical bandwidth and tuned at the 34th ITU channel. The FUT is a ∼45 m-long standard single mode fiber spool and it is interrogated with a 8 dBm probe signal. The backscattering light resulting from the propagation of the probe comb is combined with the −10 dBm LO and detected with a 100 MHz bandwidth AC balanced photodetector (BPD-AC). The LO passed through a polarization control (PC) to maximize the amplitude of the coherent detection. The detected electrical signal is low-pass filtered with a 240 kHz bandwidth, digitalized by a real-time oscilloscope (RTO) at 2.5 MS/s and processed offline only in the first Nyquist zone.

In order to directly obtain the spectral response of the fiber in the electrical domain without the need for further processing, both PRBS generators have the same sequence of N bits but are fed with two slightly different and synchronized clocks, Clk_1 and Clk_2. In this scheme, the spatial resolution will be limited by the bit-rate of the PRBS which determines the bandwidth of the frequency combs, BW. The maximum attainable range of measurement, L_{max}, will be set by the repetition rate, f_r, where $L_{max} = c/(f_r \cdot 2 \cdot n)$ and $f_r = R_b/N$. Finally, the difference between the two clocks, $\Delta f = (Clk_1\text{-}Clk_2)$, will determine the acoustic sampling of the measurement, $\delta f = \Delta f/N$.

The newly proposed generation scheme was tested with a thermo electric-cooler (TEC) that acted as a hot/cold spot. 4 cm of the FUT were placed on the top plate, together with an NTC thermistor used as a reference measurement of the temperature. The TEC was fed with an electric current controlled by a relay that switched the current polarity following a time square signal. Throughout half of the cycle, the system exhibited a temperature increase, while during the remaining half, it decreased.

For the first performance evaluation of the proposed scheme, the BW of the signal was set to 5 GHz which yields to a nominal resolution of 2 cm. The pattern length provided by the PRBS generator cards was set to 2^{14}-1 which results in a repetition rate, and thus a frequency separation between lines of $f_r = 305$ kHz. The difference between clocks, Δf, was set to 125 kHz, which yields to an acoustic sampling of $\delta f = 7.6$ Hz. In order to have the same gauge length and nominal resolution values, the digital filtering of the signal after photodetection was set to 125 kHz. In this particular context, the fiber setup employed, spanning approximately 45 meters, remained within the permissible range for these parameters (L_{max} ∼339 meters). The compression factor of the 1.45 μs trace is 40, 000, which expands the detection time of one trace up to 58 ms. In the first measurements, the current amplitude in the TEC was limited to 0.6 A while its frequency was set to 0.126 Hz.

The recovered amplitude traces are depicted in Fig. 3. In this case, the measurement was acquired for 50 seconds but, for the sake of clarity, only four traces with a four-second difference between them are represented. The inset graph depicts a zoom in a non-perturbed area of the fiber where the stability of the trace can be verified by the perfect matching between successive traces.

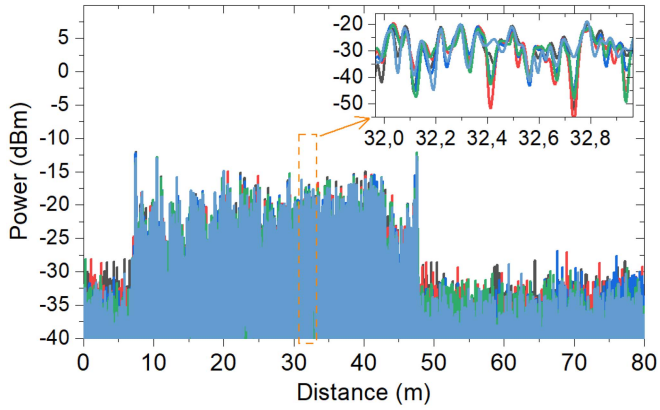

Fig. 3. Overlapped backscattered amplitude traces, measured with the common-path generation scheme. Inset depicts a zoom of an unperturbed area to illustrate the repeatability.

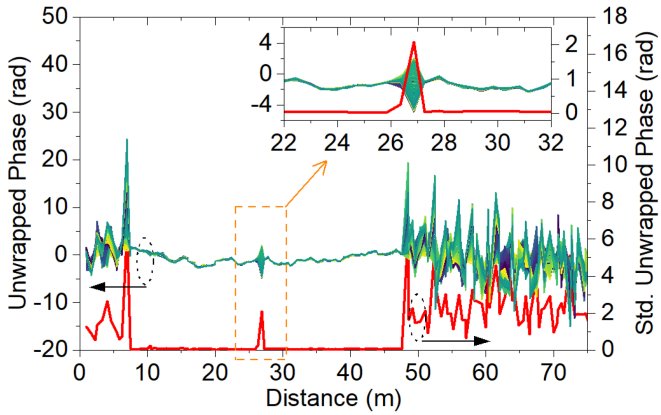

Fig. 4. Overlapped phase traces, recovered with the common-path generation scheme. Red line depicts the standard deviation of the phase values for the 50 s acquisition time. Inset depicts a zoom of the perturbed area to highlight the contrast between stimulated point and unperturbed adjacent regions.

Fig. 4 depicts the recovered phase obtained for all the 380 traces digitalized during the 50 s at a rate of $\delta f = 7.6$ Hz. Here, the phase stability can be assessed in those non-perturbed regions of the fiber where the value remains virtually constant throughout the capture time. The perturbed section can be clearly depicted at the midpoint of the fiber where the phase value rapidly changes for successive traces. At this point, the standard deviation of the recovered phase, shown in red line in Fig. 4, exhibits a value significantly higher than adjacent areas corresponding to non-stimulated zones. This allows for a precise determination of the location and extension of the perturbation.

The temporal evolution of the phase at the perturbed point, corresponding with the blue curve in Fig. 5, is in great accordance with the NTC temperature, green curve, in contrast with the phase evolution for an arbitrary non-perturbed point,

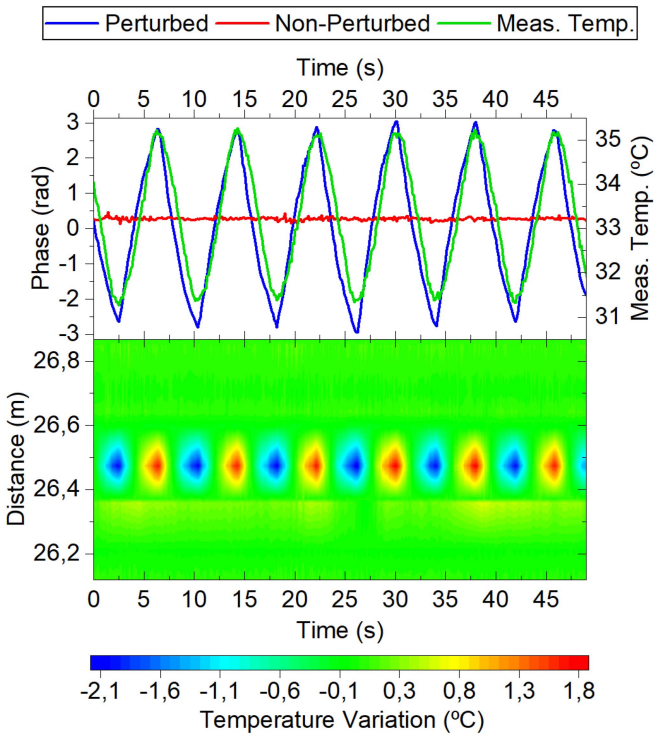

Fig. 5. Upper graph shows the evolution of the phase for the perturbed point in blue and the non-perturbed point in red. Green line presents the temperature measured with the NTC resistance. Bottom graph presents the temperature map around the perturbed area where the successive heating-cooling cycle can be observed across the hot-spot region.

red curve, that is almost constant. The temperature stimulus measured with the NTC depicts a ∼3.9 °C peak-to-peak and ∼0.13 Hz periodic signal and the recovered phase data exhibit a similar temporal evolution throughout the whole acquisition time. When comparing the perturbed and non-perturbed point, it can be clearly seen that the invariant phase in the unperturbed point reveals a high stability for the measurement period originated from the use of a common path in the generation stage in the proposed architecture.

Fig. 5 also presents the heat map, focused in the thermally perturbed region. The map is obtained from the calibration of the recovered phase trace taking account the refractive index of the employed fiber and the gauge length determined by the configuration parameters [20]. Disparities in the absolute temperature magnitude with the NTC temperature may be caused by the different position of NTC and fiber on the TEC plate. Since polarization diversity in detection has not been applied in this proof of concept test, the polarization of the LO is adjusted to avoid polarization fading within the analysis regions. Additionally, the employment of an interpolation algorithm was necessary to obtain the phase in locations with low SNR in the intensity trace attributed to destructive interference [21]. While this approach generates a homogeneous density resolution map of phase values along the entire length of the fiber, the interpolated phase at stable fading points may introduce local discontinuities in the temperature profile as it can be seen in Fig. 5 around the 26.36 m location.

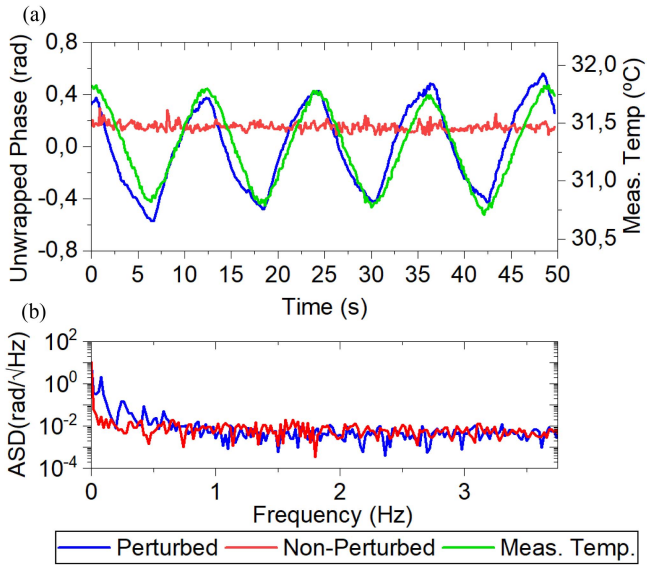

Fig. 6. Comparison of the temporal evolution of the phase for the perturbed region (blue) and unperturbed region (red) along with the measured temperature in the NTC (green) (a) in the time domain and (b) in the frequency domain.

B. Measurement Stability and Comparison Between the Two Generation Schemes

In order to evaluate the performance enhancement of the proposed architecture compared to the conventional one (i.e., based on two independent MZM interferometers for the DFC generation), the temperature stimulus was reduced to a maximum current of 0.2 A and a frequency of 0.083 Hz. These conditions were selected not only to assess the performance of the system under long-term measurement scenarios, thereby evaluating the stability enhancement derived from the common path generation stage, but also to reduce the temperature span and ensure the triangular behavior of the stimulus. This reduction in the current of the thermal electric cooler (TEC) stimulus helps avoid thermal drifts and prevents overheating or overcooling of the fiber, addressing both stability and the integrity of the measurement environment.

To further ensure the integrity of our comparison, the layout was designed to allow both generation stages to be tested with similar components, identical stimulus and equivalent Optical Signal-to-Noise Ratio (OSNR). Additionally, the same procedure for avoiding polarization fading within the analyzed fiber section is implemented in both schemes. This deliberate design choice was aimed at eliminating external influences, thereby ruling out any discrepancies in the experimental results that could be attributed to variations in the testing environment rather than to the inherent characteristics of the generation schemes themselves.

In this sub-Hz low amplitude stimulus, the recovered phase with the proposed scheme still matches the temporal evolution of the temperature value in the TEC registered with the NTC thermistor, as it is shown in Fig. 6(a). The sensitivity of the system, estimated through the median standard deviation along the unperturbed fiber in the 50 s measurement time is 0.10 rad.

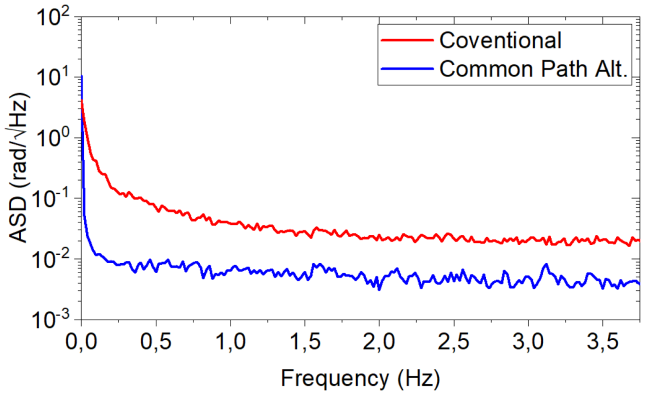

Fig. 7. Comparison in the frequency domain of the phase for unperturbed points recovered in the TE-PhiOTDR with the conventional generation scheme (red) and using the common-path generation scheme (blue).

corresponding to 0.06 K for a 2 cm gauge length. The noise analysis of the scheme has been performed considering the Amplitude Spectral Density (ASD) of the recovered phase, Fig. 6(b) The ASD for a point located in the hot/cold spot presents a prominent peak in the region of the sub-Hz which matches the present temperature variation. The other peaks observed in the blue trace are attributable to high-order harmonics, arising because the stimulus exhibits a triangular waveform. On the other hand, the ASD in a non-perturbed region presents an almost flat frequency dependence and a mean value of (0.011 ± 0.003) rad/$\sqrt{\text{Hz}}$ in the noise floor evaluated in the frequency range from 1 Hz to 3 Hz, which is considered the noise floor of the proposed scheme.

This very same scenario was measured with the conventional generation scheme and, to facilitate an equitable comparison, equivalent levels of OSNR were consistently maintained. Regarding the phase recovered with the conventional setup the average ASD noise floor (0.047 ± 0.020) rad/$\sqrt{\text{Hz}}$ with a median standard deviation value of 0.15 rad.

The ASD averaged in a section of unperturbed points within the fiber obtained for both schemes is depicted in Fig. 7 where it can be clearly seen that the proposed scheme exhibits lower ASD value for all the frequencies in the spectra when compared to the traditional generation scheme. This is a clear demonstration of the advantages of the common-path scheme. It is important to note that the sensitivity of TE-ΦOTDR can be directly compared with that of any other phase-demodulation-based ΦOTDR by just accounting for a $\sqrt{(\text{CF})}$ improvement due to the noise reduction related to the narrower detection bandwidth [13]. Moreover, the proposed common-path scheme presents a lower noise level in the low-frequency regions which provides evidence that this novel alternative scheme is advantageous for longer measurement times and reduces the instability of the conventional scheme originated from the separate generation of LO and probe combs.

IV. Conclusion

We have introduced an innovative design for the TE-ΦOTDR employing an electro-optic common path generation for both the probe and LO frequency combs. Employing a Dual-Pol IQ modulation scheme enables the creation of two polarization-orthogonal Optical Single Sideband (OSSB) signals that propagate along the same optical path without mutual interference, from the generation stage to the tested fiber. This common-path configuration significantly reduces noise from mechanical vibrations or thermal variations that could result in differential length in each branch when the signals are generated separately and then combined. This approach provides the flexibility to relocate the signal generation stage away from the tested fiber without compromising stability. Additionally, the IQ scheme introduces features such as filter-less OSSB generation, enhancing the power efficiency and integrability of the system. The system has been tested for extended-time measurements and compared to the conventional generation scheme under similar conditions and stimulus. The proposed system exhibits lower noise ASD values, especially in the low frequency region, providing evidence of the enhanced stability of this alternative scheme, especially for long-term measurement periods.

References

[1] P. Lu et al., "Distributed optical fiber sensing: Review and perspective," *Appl. Phys. Rev.*, vol. 6, no. 4, Oct. 2019, Art. no. 041302, doi: 10.1063/1.5113955.

[2] A. Barrias, J. R. Casas, and S. Villalba, "A review of distributed optical fiber sensors for civil engineering applications," *Sensors*, vol. 16, no. 5, May 2016, Art. no. 748, doi: 10.3390/s16050748.

[3] Y. Rao, Z. Wang, H. Wu, Z. Ran, and B. Han, "Recent advances in phase-sensitive optical time domain reflectometry (Φ-OTDR)," *Photonic Sensors*, vol. 11, no. 1, pp. 1–30, Mar. 2021, doi: 10.1007/s13320-021-0619-4.

[4] C. Escobar-Vera et al., "Dynamic curvature sensing using time expanded ΦOTDR," *Opt. Lett.*, vol. 48, no. 16, pp. 4336–4339, Aug. 2023, doi: 10.1364/OL.494466.

[5] G. Fang, Y. E. Li, Y. Zhao, and E. R. Martin, "Urban near-surface seismic monitoring using distributed acoustic sensing," *Geophysical Res. Lett.*, vol. 47, no. 6, 2020, Art. no. e2019GL086115, doi: 10.1029/2019GL086115.

[6] H. Wu, X. Liu, Y. Xiao, and Y. Rao, "A dynamic time sequence recognition and knowledge mining method based on the hidden Markov models (HMMs) for pipeline safety monitoring with Φ-OTDR," *J. Lightw. Technol.*, vol. 37, no. 19, pp. 4991–5000, Oct. 2019, doi: 10.1109/JLT.2019.2926745.

[7] J. C. Juarez, E. W. Maier, K. N. Choi, and H. F. Taylor, "Distributed fiber-optic intrusion sensor system," *J. Lightw. Technol.*, vol. 23, no. 6, pp. 2081–2087, Jun. 2005, doi: 10.1109/JLT.2005.849924.

[8] A. H. Hartog, *An Introduction to Distributed Optical Fibre Sensors*. Boca Raton, FL, USA: CRC Press, 2017, doi: 10.1201/9781315119014.

[9] H. Izumita, S.-I. Furukawa, Y. Koyamada, and I. Sankawa, "Fading noise reduction in coherent OTDR," *IEEE Photon. Technol. Lett.*, vol. 4, no. 2, pp. 201–203, Feb. 1992, doi: 10.1109/68.122361.

[10] H. F. Martins, S. Martin-Lopez, P. Corredera, P. Salgado, O. Frazão, and M. González-Herráez, "Modulation instability-induced fading in phase-sensitive optical time-domain reflectometry," *Opt. Lett.*, vol. 38, no. 6, pp. 872–874, Mar. 2013, doi: 10.1364/OL.38.000872.

[11] W. Zou, S. Yang, X. Long, and J. Chen, "Optical pulse compression reflectometry: Proposal and proof-of-concept experiment," *Opt. Exp.*, vol. 23, no. 1, pp. 512–522, Jan. 2015, doi: 10.1364/OE.23.000512.

[12] B. Lu et al., "High spatial resolution phase-sensitive optical time domain reflectometer with a frequency-swept pulse," *Opt. Lett.*, vol. 42, no. 3, pp. 391–394, Feb. 2017, doi: 10.1364/OL.42.000391.

[13] M. Soriano-Amat et al., "Time-expanded phase-sensitive optical time-domain reflectometry," *Light Sci. Appl.*, vol. 10, no. 1, Mar. 2021, Art. no. 51, doi: 10.1038/s41377-021-00490-0.

[14] M. Soriano-Amat et al., "Millimetric spatial resolution time-expanded ϕ-OTDR," *APL Photon.*, vol. 8, no. 10, Oct. 2023, Art. no. 100803, doi: 10.1063/5.0150991.

[15] M. Soriano-Amat, H. F. Martins, V. Durán, S. Martin-Lopez, M. Gonzalez-Herraez, and M. R. Fernández-Ruiz, "Quadratic phase coding for SNR improvement in time-expanded phase-sensitive OTDR," *Opt. Lett.*, vol. 46, no. 17, pp. 4406–4409, Sep. 2021, doi: 10.1364/OL.432350.
[16] J. Preciado-Garbayo et al., "Time-expanded Φ-OTDR based on binary sequences," *IEEE Photon. Technol. Lett.*, vol. 34, no. 13, pp. 695–698, Jul. 2022, doi: 10.1109/LPT.2022.3181819.
[17] M. Tapiador et al., "Definition of a FPGA-based SoC architecture for PRBS transmission in optical spectroscopy," *IEEE Trans. Instrum. Meas.*, vol. 72, 2023, Art. no. 2007109, doi: 10.1109/TIM.2023.3315366.
[18] C. Deakin and Z. Liu, "Noise and distortion analysis of dual frequency comb photonic RF channelizers," *Opt. Exp.*, vol. 28, no. 26, pp. 39750–39769, Dec. 2020, doi: 10.1364/OE.410340.
[19] P. Sevillano, J. Preciado-Garbayo, D. Izquierdo, S. Martin-Lopez, M. Gonzalez-Herraez, and M. R. Fernández-Ruiz, "Time-expanded ΦOTDR based on orthogonal polarization frequency comb generation," in *Proc. 28th Int. Conf. Opt. Fiber Sensors*, 2023, Paper Tu2.4, doi: 10.1364/OFS.2023.Tu2.4.
[20] Y. Koyamada, M. Imahama, K. Kubota, and K. Hogari, "Fiber-optic distributed strain and temperature sensing with very high measurand resolution over long range using coherent OTDR," *J. Lightw. Technol.*, vol. 27, no. 9, pp. 1142–1146, May 2009, doi: 10.1109/JLT.2008.928957.
[21] J. Zhou, Z. Pan, Q. Ye, H. Cai, R. Qu, and Z. Fang, "Characteristics and explanations of interference fading of a \phi -OTDR with a multi-frequency source," *J. Lightw. Technol.*, vol. 31, no. 17, pp. 2947–2954, Sep. 2013, doi: 10.1109/JLT.2013.2275179.

Pascual Sevillano received the M.Sc. and Ph.D. degrees in physics from the University of Zaragoza, Zaragoza, Spain, in 2010 and 2015, respectively. From 2015 to 2020, he was with Aragon Photonics Labs, where he was the Head of the Research and Development Department. In late 2020, he joined the Department of Applied Physics, University of Zaragoza, as an Assistant Professor. In 2021, he becomes a member of the Engineering Research Institute of Aragon (I3A). His research interests include no-linear optical phenomena in fiber and its application in distributed sensing.

Javier Preciado-Garbayo received the bachelor's degree in telecomunications technology and services engineering and the master's degree in telecommunications engineering from the University of Zaragoza, Zaragoza, Spain, in 2015 and 2017, respectively, and the industrial Ph.D. degree focused on distributed optical fiber sensors "Integración de sistemas de sensado distribuido sobre fibra óptica y estudio de aplicaciones de uso" from the company Aragon Photonics Labs, Spain, in 2023.During the second year of the master's degree, he was part of Erasmus exchange program in Linköping University, Linköping, Sweden. He is a Technical Leader with the Sensing Division, Aragon Photonics Labs.

David Izquierdo received the M.Eng. and Ph.D. degrees in telecommunications from the University of Zaragoza, Zaragoza, Spain, in 2004 and 2011, respectively. From 2013 to 2022, he was an Associate Professor with Centro Universitario de la Defensa. He is currently with the Department of Applied Physics, University of Zaragoza, as an Assistant Professor. His research interests include integrated photonics, coherent optical communications, photonic characterization and sensing instrumentation, and broadband communications systems.

Miguel Soriano-Amat received the bachelor's degree in physics and the master's degrees in advanced physics from the Universitat de València, Valencia, Spain, in 2017 and 2018, respectively, and the Ph.D. degree in electronics from the Universidad de Alcalá, Alcalá de Henares, Spain, in 2023. He is a Postdoctoral Researcher with the Photonics Engineering Group, University of Alcalá. His research focuses on the developing of high-resolution distributed acoustic sensors based on optical frequency combs.

Sonia Martin-Lopez (Member, IEEE) received the Ph.D. degree from the Universidad Complutense de Madrid, Madrid, Spain, in 2006. She had a Predoctoral stay with the Nanophotonics and Metrology Laboratory, Ecole Polytechnique Federale de Lausanne, Lausanne, Switzerland. She has been involved as a Postdoctoral Researcher with Applied Physics Institute and Optics Institute, Spanish Council for Research, Madrid, for six years. She is currently an Associate Professor with the Photonics Engineering Group, University of Alcalá, Alcalá de Henares, Spain. She has authored or coauthored more than 200 papers in international refereed journals and conference contributions. Her research interests include nonlinear fiber optics and distributed optical fiber sensors.

Miguel Gonzalez-Herraez (Senior Member, IEEE) received the D.Eng. degree in telecommunications engineering from Universidad Politécnica de Madrid, Madrid, Spain, in 2004. Since 2004, he has been with the Department of Electronics, University of Alcalá, Alcalá de Henares, Spain, where he is currently a Full Professor. He has authored or coauthored more than 300 research articles in indexed journals and contributions to prestigious international conferences in the field of photonics. His research interests include distributed optical fiber sensing, nonlinear fiber optics, and ultrafast fiber lasers. Dr. Gonzalez-Herraez is a Senior Member of the Optical Society of America. He is an Associate Editor of IEEE PHOTONICS TECHNOLOGY LETTERS.

María R. Fernández-Ruiz received the M.Eng. degree in telecommunications and the M.Sc. degree in electronics and signal processing from the University of Seville, Seville, Spain, in 2009 and 2011, respectively, and the Ph.D. degree in telecommunications from the University of Quebec, Montreal, QC, Canada, in 2016. She is currently a Ramon y Cajal Postdoctoral Researcher with the Photonics Engineering Group, University of Alcalá, Alcalá de Henares, Spain. She has authored or coauthored more than 100 papers in international refereed journals and conference contributions. Her current research interests include optical signal processors, nonlinear optics, and distributed optical sensors. Her research interests include the development of new architectures and applications for distributed acoustic sensor systems.